2D/3D SIMULATIONS OF BLACK-SILICON INTERDIGITATED BACK-CONTACTED c-Si(n) SOLAR CELLS

E. Calle[1], D.Carrió[1], P.Ortega[1], G. Von Gastrow[2], H. Savin[2], I. Martín[1], R. Alcubilla[1]

[1] Universitat Politècnica de Catalunya, Micro and Nano Technologies Group MNT,.
C/ Jordi Girona 1-3, Mòdul C4, 08034 Barcelona, Spain, pho. +34 934054193, e.mail: eric.calle@upc.edu
[2] Aalto University, Department of Electronics and Nanoengineering Tietotie 3, 02150 Espoo, Finland
e-mail: hele.savin@aalto.fi

ABSTRACT: black silicon (b-Si) reduces drastically light reflectance in the front side of c-Si solar cells to values near zero for the whole absorbed solar spectrum. In this work, we apply 2D and 3D simulations to explore the efficiency limits of interdigitated back-contacted c-Si(n) solar cells with line or point contacts respectively, using ALD Al_2O_3 passivated b-Si in the front surface. Realistic physical and technological parameters involved in a conventional oven-based fabrication process are considered in the simulations, especially those related to surface recombination on the b-Si as well as high doped p+/n+ strip regions. One important issue is the temporal stability of surface passivation on b-Si surfaces. In this work experimental long-term b-Si surface passivation data after two years and its impact on cell performance are studied. Simulations demonstrate initial and final photovoltaic efficiencies over 24.6% and 23.2% respectively for an emitter coverage of 80% independently of the cell contact strategy. A photocurrent loss about 1.3 mA/cm^2 occurs when surface recombination velocity at the b-Si surfaces degrades from 6 cm/s to a final value of 28 cm/s.
Keywords: c-Si, 3D simulations, black-silicon, IBC solar cell, point-like contacts, surface passivation

1 INTRODUCTION

Nano-textured silicon, also referred as black silicon (b-Si), is an excellent choice to drastically reduce crystalline Si solar cell reflectance in the useful solar spectrum [1]. One of the major issues related to b-Si surfaces is the possible increase of surface/bulk recombination due partly to the enlarged surface area of such nanostructures and partly to a possible lattice damage during etching. These drawbacks have been overcome successfully in the last years applying less aggressive etching techniques based on inductively-couple plasma reactive ion etching (ICP-RIE) combined with surface passivation based on atomic layer deposited (ALD) Al_2O_3 films. Thereby, effective surface recombination velocities (S_{eff}) below 10 cm/s on p- and n-type c-Si substrates have been achieved [2-5]. Black silicon surfaces passivated by Al_2O_3 have been used either in front-back-contact or all-back-contact solar cells [6-8]. In particular, Interdigitated Back Contacted (IBC) architecture is very well suited to b-Si. In this cell structure, the front surface passivation and antireflection coating are totally decoupled from the rear electrodes design. Recently IBC cells with b-Si front surface, from now on b-Si IBC cells, have reached promising efficiencies beyond 22% independently of substrate polarity [9, 10]. One important issue related to b-Si is the temporal stability of surface passivation. In a previous work we have reported long-term degradation of S_{eff} parameter on b-Si surfaces both for n- and p-type substrates [5], but its impact in the IBC cell photovoltaic performance is not explored yet.

In this work, we study the long-term efficiency potential of ALD Al_2O_3 passivated b-Si IBC c-Si(n) cells as well as the influence of the cell geometry, i.e. emitter coverage (f_e), in the photovoltaic performance by means of 2D/3D simulations (Synopsys Sentaurus Device). Realistic physical parameters for front and rear surfaces are considered in the simulations based on separate experimental recombination lifetime measurements. Two types of structures are simulated: IBC cells with contact lines (2D) and alternatively using locally point square contacts (3D).

2 CELL DEFINITION AND OPTICAL MODEL

2.1 Unit cell geometry definition

Solar cells are large area devices but symmetrical enough to be studied as a repetition of a simple domain or unit cell, reducing simulation time and hardware computational requirements. The corresponding IBC solar cell is a periodical repetition of the unit cell, once it is flipped respect to the symmetry axis, with a periodicity related to the contact pitch in the x and y directions. In fig. 1 the simplest unit cell for the 3D and 2D IBC c-Si(n) solar cell architectures are shown. Notice that the p+ emitter is partly passivated with ALD Al_2O_3 and the rest with thermal SiO_2. In this way the electrical behavior of the whole structure can be obtained considering that each unit cell is electrically connected in parallel with the others (current scaling up).

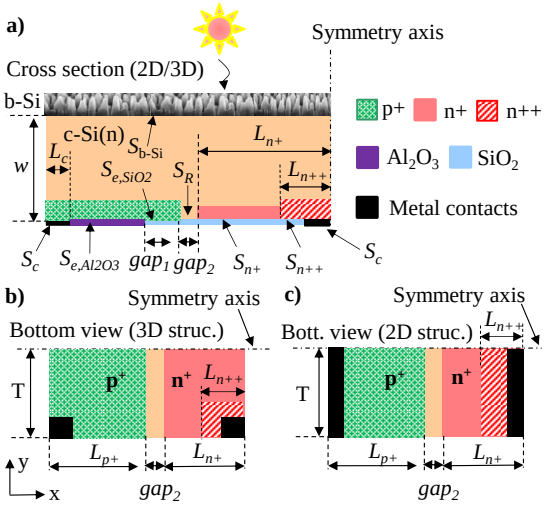

Figure 1: a) 2D cross section sketch of the simplest unit cell, with only one base and one emitter contacts, is shown. b) and c) bottom views for the 3D and 2D unit cells considering point-like and line-like contacts respectively.

Notice that the unit cell contains only the half area of a single emitter and base contacts and strip p+ and n+ doped regions are used in the simulations. Additionally, we include square and strip n++ regions beneath electron contacts in the 3D and 2D simulations respectively.

Table I summarizes the geometrical values as well as the parameters related to doped regions used in the study. Gaussian doping profiles are introduced in the simulations considering the expected surface doping N_s and the sheet resistance R_{sh} for each doped region using our convectional fabrication process. Notice that changing the length of p+ regions (L_{p+}), from 98 to 798 µm and fixing the other length parameters, the emitter coverage f_e ranges from 50 to 89%.

Table I: Geometrical and doping profile parameter values.

Geometrical parameters (µm)							
w	T	gap_1	gap_2	L_{n+}	L_{n++}	L_{p+}	L_c 3D/2D
260	100	98(*)	4	98	50	98-798	25/15
Doping profile parameters							
$N_{s,n++}$ (cm^{-3})	$R_{sh,n++}$ (Ω/sq)	$N_{s,n+}$ (cm^{-3})	$R_{sh,n+}$ (Ω/sq)	$N_{s,p+}$ (cm^{-3})	$R_{sh,p+}$ (Ω/sq)		
7×10^{19}	7.0	3.5×10^{18}	110	5×10^{18}	190		

(*) For L_{p+}-L_c<100 µm then $gap_1=L_{p+}$ - L_c

2.2 Optical model

Optical modelling of b-Si surfaces is quite complex in general. However, we can use a good approach to simulate the photogeneration inside the structure from experimental reflectance data as follows: 1) a modified AM1.5G solar spectral irradiance is introduced in the simulations (I_{mod}) considering the measured reflectance of b-Si coated with 20 nm thick ALD Al_2O_3 layer ($R_{b\text{-}Si}$) as $I_{mod}=I_{AM1.5}(1-R_{b\text{-}Si})$ (see Fig.2). 2) Total photon transmission (T=100%) and internal front reflectance (R_{int_Front}=100%). 3) An average internal rear reflectance (<R_{int_rear}>) is assumed in the simulations taking into account contacted, metalized and non-metallized non-contacted areas with local reflectance of 75, 96 and 85% respectively. 4) Ray tracing is performed using for absorption and refractive index the default wavelength dependent program values for c-Si.

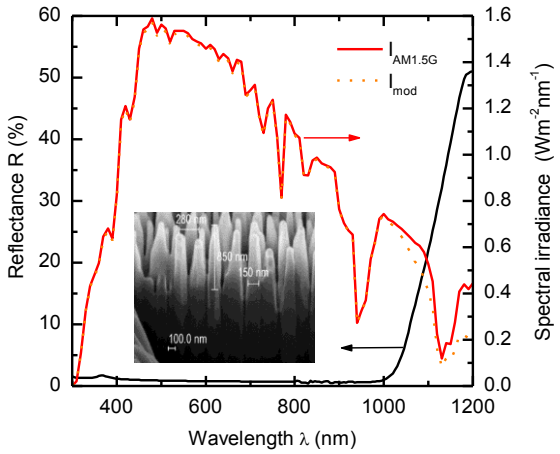

Figure 2: b-Si reflectance (sample coated with 20 nm thick ALD Al_2O_3 layer), AM1.5G and modified spectral irradiances used in the simulations. A SEM/FIB image of the b-Si surface is also shown in the inset.

The simplified simulated structure, from an optical point of view, is shown in Fig. 3 where gap_{metal} is the distance between electron and hole metal electrodes, 80 µm in our devices.

Flat energy bands have been considered at the passivated semiconductor surfaces. Therefore, there are no inversion or accumulation layers below passivated surfaces. Additionally, physical models, e.g. carrier statistics, band gap narrowing, and carrier mobilities are the same as considered in [11].

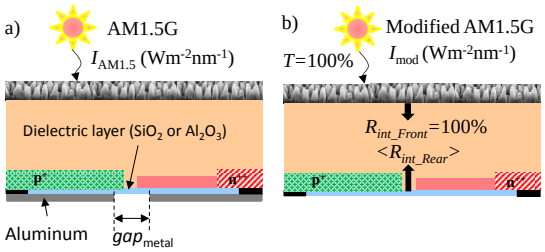

Figure 3: a) Cross section of a b-Si IBC cell and b) its equivalent structure considering the simplified optical model.

3 SURFACE RECOMBINATION

In order to have accurate simulations is important to introduce realistic surface recombination velocities values (S) at the different surface regions of the IBC device. In this section, we determine these parameters evaluated in the b-Si surface as well as in the p+, n+ and n++ doped regions. Experimental symmetrical test samples using high quality c-Si (n/p) FZ <100> substrates (270 µm thick and 2 ± 1 Ωcm) were prepared to perform effective lifetime (τ_{eff}) measurements by the QSS-PC technique.

3.1 Surface recombination at b-Si surfaces

The most critical parameter in the IBC simulations is the surface recombination velocity at the nanostructured surface ($S_{b\text{-}Si}$). In Figure 4 $S_{b\text{-}Si}$ values, once b-Si surfaces are passivated with 20 nm ALD Al_2O_3, are extracted from τ_{eff} data on c-Si(n) substrates considering a time window study of two years. Experimental details are reported in [5]. Surface recombination velocities are calculated using eq. (1) and evaluated at a carrier excess density of $\Delta n=10^{15}$ cm^{-3}, being w the sample thickness. In this study we consider that bulk lifetime is dominated by intrinsic recombination mechanisms (auger and band-to-band), being τ_{in} the related lifetime, using Richter et al parameterization [12]. b-Si data are directly compared with random pyramids textured surfaces passivated with the same Al_2O_3 layer as a reference.

$$S_{b-Si} \cong \frac{w}{2}\times\left(\frac{1}{\tau_{eff}}-\frac{1}{\tau_{in}}\right) \quad (1)$$

As it can be seen in Fig. 4, excellent initial $S_{b\text{-}Si}$ values extracted about 6 cm/s are achieved in the nanostructures despite the unfavorable large b-Si surface area. However this value increases after two years to 28 cm/s.

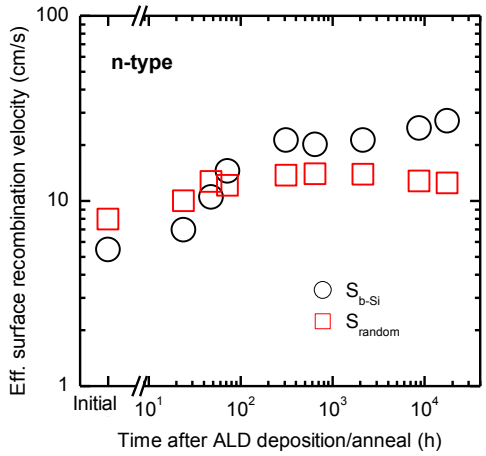

Figure 4: Surface recombination velocities for b-Si ($S_{b\text{-}Si}$) and random pyramids (S_{random}) textured surfaces on n-type substrates.

3.2 Surface recombination at p+ and n+/n++ surfaces

Surface passivation at the doped regions was determined by the extraction of the emitter recombination current density J_{oe} parameter from τ_{eff} measurements using eq. (2). Where n_i, q, and N_{bulk} are the intrisic concentration (8.56×10^9 cm^{-3} at T=25°C), q the elementary charge and N_{bulk} the bulk doping respectively. Notice that n- or p-type substrates were used to form p+ and n+/n++ emitters respectively.

$$\frac{1}{\tau_{eff}}-\frac{1}{\tau_{in}}\cong\frac{2J_{oe}}{qn_i^2w}\left(N_{bulk}+\Delta n\right) \qquad (2)$$

Samples were doped at different temperatures using solid dopant sources and underwent a drive-in stage at 1080ºC during one hour in pure O_2 ambient growing a thermal SiO_2 film of 110 nm as a passivation layer. Final emitter sheet resistance (R_{sh}) covers a range between 60-600 and 6-200 Ω/sq in boron and phosphorous doped emitters respectively. Finally, an annealing in forming gas during 10 min was made in all samples. For the boron emitters, the SiO_2 layer was removed and replaced by an ALD Al_2O_3 film deposited at 200ºC (30 nm thick) as alternative passivation layer. In this case, an extra annealing at 400ºC 10 min was made to activate surface pasivation.

In Figure 5 J_{oe} data vs. R_{sh} for phosphorous emitters are shown. Filled symbols and empty symbols correspond to passivated annealed and unpassivated (bare) n+ emitters respectively. Lines correspond with PC1D simulations considering the fundamental surface recombination velocity for holes (S_{po}) as a free simulation parameter. In that case doping profiles introduced in the PC1D program were generated using SUPREM program in agreement with the diffusion and drive-in stages followed in our test devices. As can be seen in Fig. 5, SiO_2 passivated n+ emitters follows the expected trend, i.e. the lower R_{sh} the higer J_{oe} value. The estimation of the S_{po} parameter from eq. (3) as a function of the phosphorous doping at the surface N_s allows a close fitting of the J_{oe} values, as it is already reported in the literature [13].

Experimental J_{oe} data meaured in boron doped emitters are shown in Fig. 6. ALD Al_2O_3 films offer a better performance than SiO_2 passivated boron emitters in the whole R_{sh} range, being the fundamental surface recombination velocity for electrons (S_{no}) around 200 cm/s for a 100-200 Ω/sq emitter, much lower than its counterpart using SiO_2 as a passivated layer (1500 cm/s).

$$S_{po}=100\times\frac{N_s}{10^{18}} \qquad (3)$$

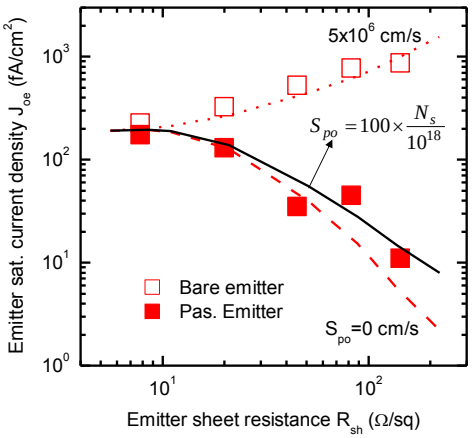

Figure 5: J_{oe} vs. R_{sh} for passivated (fill symbols) and unpassivated bare (empty symbols) phosphorous emitters. Lines correspond with PC1D/SUPREM simulations considering S_{po} as a free simulation parameter.

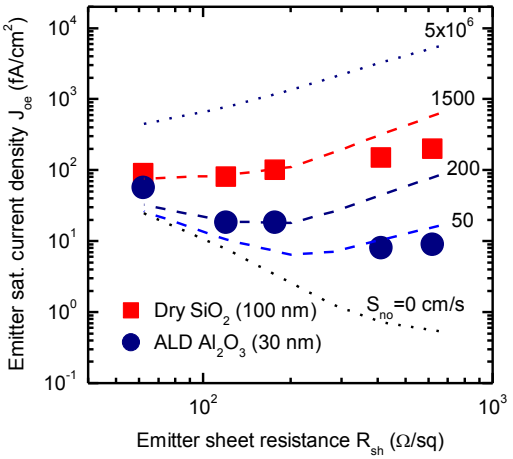

Figure 6: J_{oe} vs. R_{sh} for passivated boron emitters. Square and circles symbols correspond with passivated emitters with thermal SiO_2 and ALD Al_2O_3 respectively. Lines correspond with PC1D/SUPREM simulations considering S_{no} as a free simulation parameter.

Finally, table II summarizes all surface recombination velocities used in the 2D/3D simulations. Notice that surface recombination velocities on n+ and n++ regions are calculated taking into account eq. (3) with the surface doping given in table I.

Table II: Surface recombination velocities at the different device regions (see Fig. 1). Fundamental surface recombination velocities are considered the same in the simulations, i.e. $S_{no}=S_{po}=S_i$, in all cases.

Surface recombination velocities ($S_{no}=S_{po}$) (cm/s)					
$S_{e,Al2O3}$	$S_{e,SiO2}$	S_{n+}	S_{n++}	$S_{b\text{-}Si}$	S_R
200	1500	400	7000	6-28	10

4 b-Si IBC SOLAR CELL SIMULATION RESULTS

Simulation results for 2D and 3D b-Si IBC structures under AM1.5G solar spectrum (1 kW/m^2, T=25ºC) are shown in Fig. 7. Excellent initial efficiencies (η) up to 24.7% for emitter coverages around 80% independently of structure typology are achieved. The efficiency is limited mostly by the relatively low open circuit voltage (V_{oc}) values < 710 mV reached using our baseline fabrication process compared with the state-of-the-art around 750 mV obtained in silicon heterojunction based IBC c-Si(n) solar cells [14].

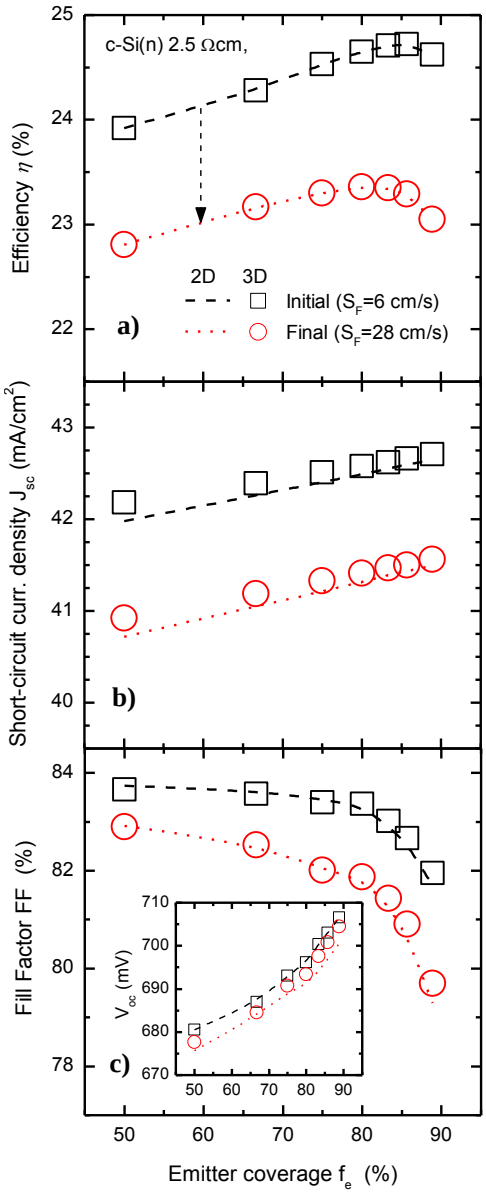

Figure 7: a) efficiency, b) short-circuit current density, and c) fill factor vs. emitter coverage for the 2D (lines) and 3D (symbols) of simulated b-Si IBC solar cells. Expected open circuit voltages are also shown in the inset of plot c).

A drop of 1.5% in absolute efficiency is expected after two years, due in part to a degradation of short-circuit current density (J_{sc}) of ~1.2 mA/cm^2 from outstanding initial and stabilized values of 42.7 and 41.5 mA/cm^2 respectively. The efficiency trend with f_e is the expected behaviour considering a trade-off between recombination and series resistance losses, i.e. higher f_e values leads to lower recombination losses, higher J_{sc} and V_{oc}, but higher ohmic losses, i.e. lower fill factors (*FF*).

5 CONCLUSIONS

In this work, we apply 2D/3D simulations to explore efficiency limits of black silicon IBC solar cells using realistic physical and technological parameters involved in a conventional oven-based fabrication process. One important issue is the temporal stability of surface passivation on b-Si surfaces. In this work long-term b-Si surface passivation and its impact on cell performance is studied. Simulations demonstrates initial and final (after two years) photovoltaic efficiencies over 24.6% and 23.2% respectively for an emitter coverage of 80% independently of the cell contact strategy. A photocurrent loss about 1.3 mA/cm^2 occurs when surface recombination velocity at the b-Si surfaces changes from 6 cm/s to a final stabilized values around 28 cm/s.

ACKNOWLEDGMENTS

This work was partially funded by the Spanish MINECO (PCIN-2014-055) and Finnish TEKES (40329/14) agencies under Solar-Era.Net FP7 European Network. Part of the work was also supported by the project REFER COMRDI15-1-0036 funded by ACCIÓ and European Regional Development Fund (FEDER) as well as the Spanish MINECO projects (ENE2016-78933-C4-1-R and TEC2014-59736-R).

REFERENCES

[1] M. Algasinger et al, *Advanced Energy Materials* 2013, **3**; 1068-1074.
[2] T. Allen et al, *In Proc. of 40th IEEE Photovoltaic Specialist Conference* 2014, Denver Colorado USA, pp. 562-566.
[3] P. Repo et al, *IEEE Journal of Photovoltaics* 2013, **3**(1); 90-94.
[4] G. von Gastrow et al, *Solar Energy Materials & Solar Cells* 2015, **142**; 29-33.
[5] E. Calle et al, *Energy procedia* 2016, **92**; 341-346.
[6] M. Otto et al, *Advanced Optical Materials* 2015, **3**; 147-164.
[7] J. Oh et al, *Nature Nanotechnology* 2012, **7**; 743-748.
[8] S. Jeong et al, *Nature Communications* 2013, **3**, doi:10.1038/ncomms3950.
[9] H. Savin et al, *Nature Nanotechnology* 2015, **10**; 624-628.
[10] P. Ortega et al, *Progress in Photovoltaics: Research and Applications* 2015, **23**(11); 1448-1457.
[11] J.M. López-González et al, *Progress in Photovoltaics: Research and Applications* 2015; **23**(1); 69-77.
[12] A. Richter et al, *Physical Review B* **86**: 165202 (2012).
[13] A. Cuevas et al, *Progress in Photovoltaics: Research and Applications* 2000; **8**(6); 603-616.
[14] K. Masuko et al, *IEEE Journal of Photovoltaics* 2014; **4**(6); 1433-1435.